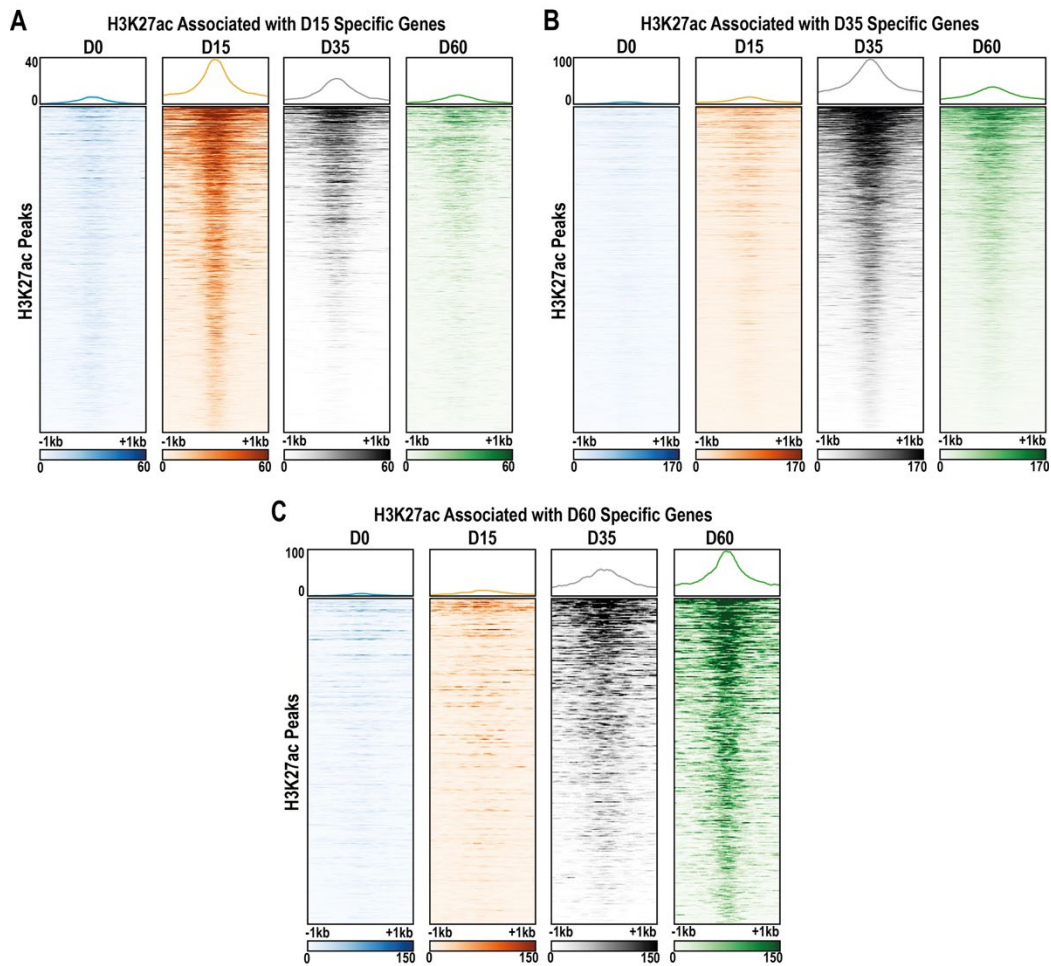**Supplemental information**

Defining cis-regulatory elements

and transcription factors that control

human cortical interneuron development

Gareth Chapman, Julianna Determan, Haley Jetter, Komal Kaushik, Ramachandran Prakasam, and Kristen L. Kroll

Supplementary Figures

Figure S1. Changes in H3K27ac enrichment at peaks associated with genes with stage-specific expression, Related to Figure 2. Representative heat maps of H3K27ac peaks within 20 kb of the nearest TSS associated with genes with D15 (**A**), D35 (**B**) or D60 (**C**) specific expression, showing a 2 kb region around the center of each peak. Color intensities and Y axis scales are representative of read depth normalized per 10 million reads.
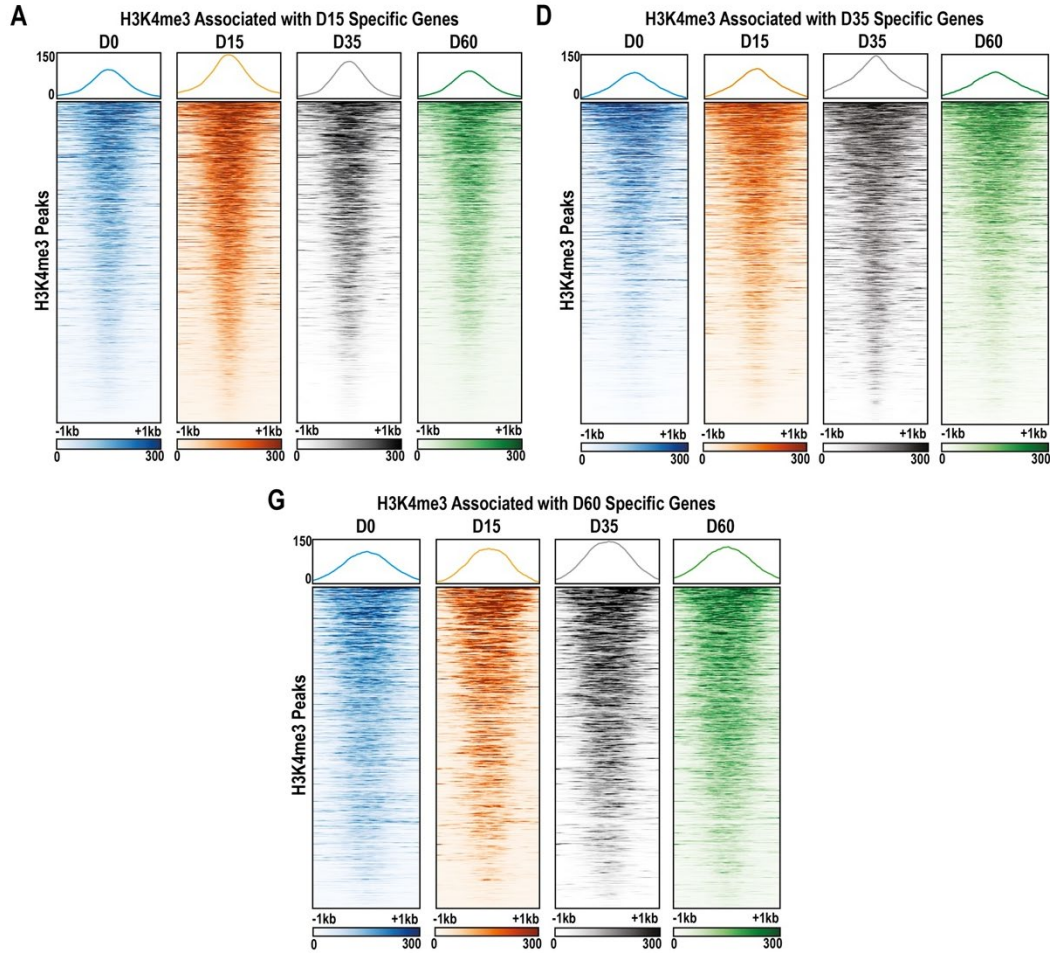
Figure S2. Changes in H3K4me3 enrichment at peaks associated with genes with stage-specific expression, Related to Figure 2. Heat maps of H3K4me3 peaks within 20 kb of the nearest TSS associated with genes with D15 (**A**), D35 (**B**) or D60 (**C**) specific expression, showing a 2 kb region around the center of each peak. Color intensities and Y axis scales are representative of read depth normalized per 10 million reads.
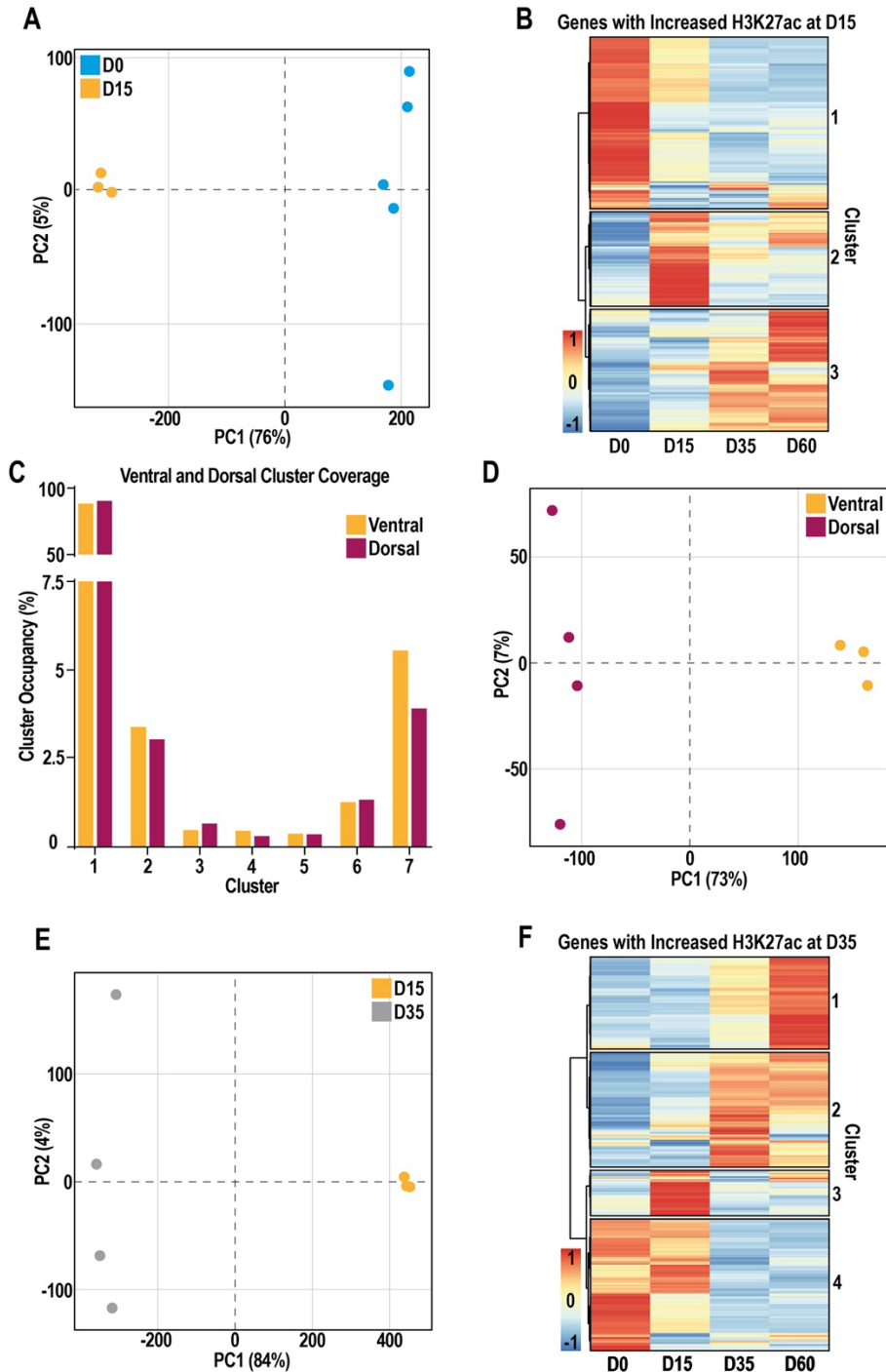
Figure S3. Significant changes in H3K27ac enrichment during interneuron differentiation, Related to Figure 3. (**A**) Principal component analysis of D0 (Blue, N=5) and D15 (Orange, N=3) H3K27ac peaks. (**B**) Hierarchical clustering of expression of genes associated with a significant increase of H3K27ac signal at D15 by comparison with D0. (**C**) Comparison of chromatin state occupancy (as defined by our ChromHMM model) between dorsal telencephalic-patterned neuronal progenitors (Purple, N=4) versus MGE-like ventral telencephalic-patterned progenitors (Orange, N=3). (**D**) Principal component analysis of H3K27ac peaks in dorsal telencephalic patterned neuronal progenitors (Purple) and MGE-like ventral telencephalic patterned progenitors (Orange). (**E**) Principal component analysis of H3K27ac peaks at D15 (Orange, N=3) versus D35 (Grey, N=4). (**F**) Hierarchical clustering of expression of genes associated with a significant increase in H3K27ac signal at D35 versus D15.

3
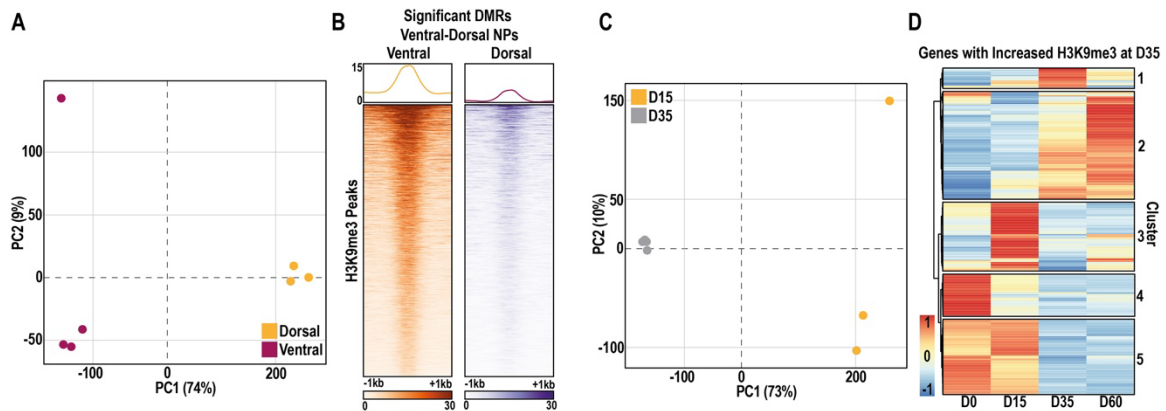
Figure S4. **Significant changes in H3K9me3 enrichment during interneuron differentiation, Related to Figure 3.** (**A**) Principal component analysis of H3K9me3 peaks in dorsal telencephalic patterned neuronal progenitors (Purple, N=4) and MGE-like ventral telencephalic patterned progenitors (Orange, N=3). (**B**) Heat maps of H3K9me3 peaks with significantly increased signal in MGE-like ventral telencephalic patterned progenitors (Orange) versus dorsal telencephalic patterned neuronal progenitors (Purple). Color intensities and Y axis scales for heat maps of H3K9me3 signal are representative of read depth normalized per 10 million reads. (**C**) Principal component analysis of D15 (Orange, N=3) and D35 (Grey, N=4) H3K9me3 peaks. (**D**) Hierarchical clustering of genes associated with a significant increase of H3K9me3 signal at D35 compared to D15.
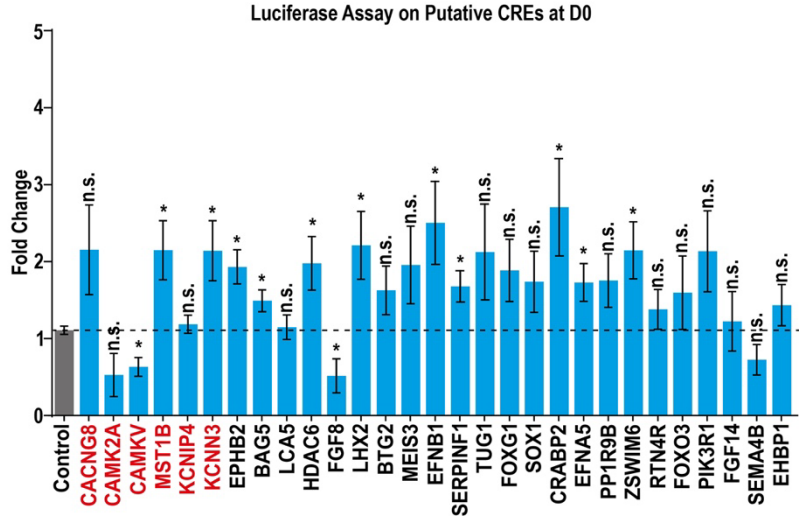
Figure S5. Functional assessment of CRE-luciferase reporter plasmids in D0 hESCs, Related to Figure 4. Luminescence in D0 hESCs transfected with luciferase reporters containing CREs, normalized to the same luciferase vector without a CRE. Dotted line represents fold change, by comparison with the empty vector with no CRE (basal expression) CREs labelled in red contain an RFX binding motif. Data was analyzed with the Students T-Test compared to empty vector, *pValue<0.05 and N=4. n.s.=not significant.
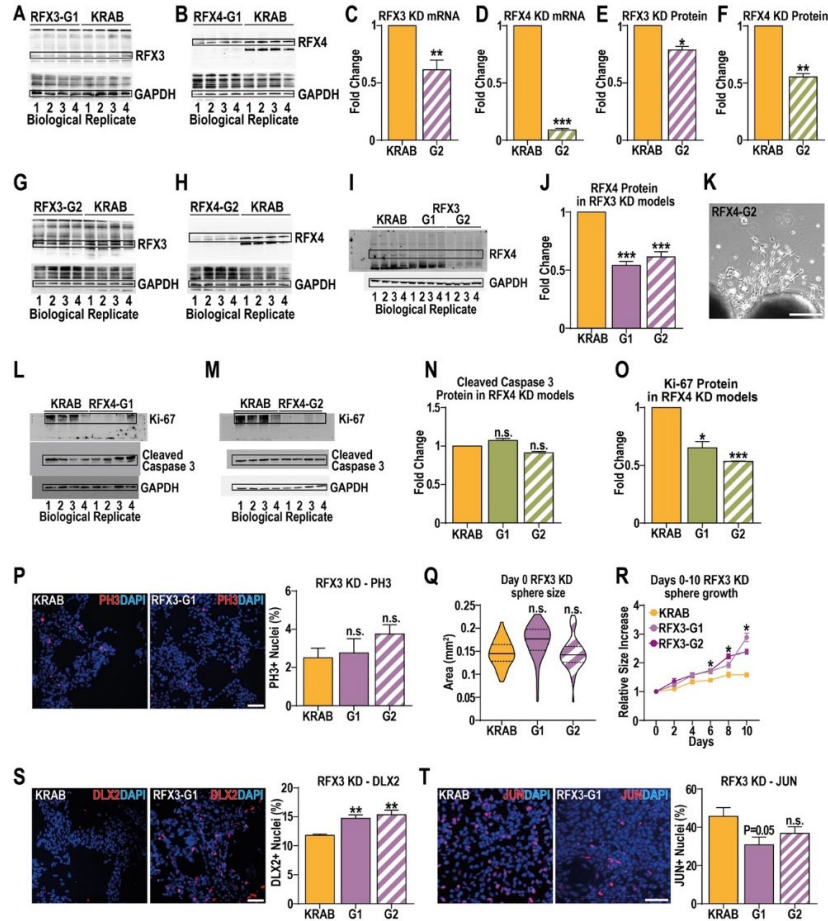
Figure S6. Characterization of RFX3 and RFX4 KD models, Related to Figure 5. (A-B) Western blots for (**A**) RFX3 and (**B**) RFX4 in the KRAB and RFX3-G1 or RFX4-G1 KD models in D15 ventrally patterned neuronal progenitors; predicted RFX3, RFX4, and GAPDH bands are indicated, based on known molecular weight. (**C-F**) Changes in (**C-D**) mRNA and (**E-F**) protein levels of RFX3 or RFX4 in the (**C, E**) RFX3-G2 or (**D, F**) RFX4-G2 knockdown models in D15 ventrally patterned neuronal progenitors. (**G-H**) Western blots for (**G**) RFX3 and (**H**) RFX4 in the KRAB and RFX3-G2 or RFX4-G2 KD models, with predicted RFX3, RFX4, and GAPDH bands indicated, based on known molecular weight. (**I**) Western blot for RFX4 in the KRAB and RFX3 KD models with predicted RFX4 and GAPDH bands indicated based on known molecular weight, and (**J**) quantification of changes in RFX4 protein expression in RFX3 KD models. (**K**) Example image of neuronal morphology during D12 outgrowth from RFX4-G2 KD neurospheres. Scale bar=100 μm. (**L-M**) Western blots for Ki-67 and cleaved caspase 3 in (**L**) RFX4-G1 and (**M**) RFX4-G2 and paired KRAB control models at D12 of differentiation; predicted Ki-67, cleaved caspase 3, and GAPDH bands are indicated, based on known molecular weight. (**N-O**) Changes in the protein levels of (**N**) cleaved caspase 3 and (**O**) Ki-67 in RFX4 KD models, relative to the KRAB control. (**P**) Example images and quantifications for the proportion of cells that were immunopositive for phosphorylated histone H3 (PH3) in the KRAB and RFX3 KD models. (**Q**) Quantification of sphere size in the RFX3 KD and KRAB models on D0 of differentiation and (**R**) changes in sphere size in the RFX3 KD and KRAB models from D0-D10 of differentiation, normalized to the average sphere size of each biological replicate in each model at D0 of differentiation. (**S**) Representative images and quantification of the proportion of cells that were immunopositive for DLX2 in the KRAB and RFX3 KD models. (**T**) Representative images and quantification of the proportion of cells that stained positive for JUN in the KRAB and RFX3 KD models. Data is represented as mean +/- SEM. C-F, J, N-O, P-Q and R-T was analyzed using a Students T-Test, comparing to the KRAB controls *pValue<0.05, **pValue<0.01 and ***pValue<0.001. R was analyzed using a two way anova with Dunnett;s multiple comparison testing *pValue<0.05 in both RFX3 KD models compared to KRAB. N=4 for all conditions and scale bar=50 μm.